Dynamic and Ballistic Analysis of the SpinLaunch Accelerator

Rajat Gupta
ROB-GY 7863: Autonomous Space Robotics, Fall 2025
New York University, Tandon School of Engineering

***Abstract*—This analysis investigates the critical factors determining the feasibility of the SpinLaunch centrifugal mass accelerator, focusing on structural stability and optimizing the angle of throw. We quantify the centripetal acceleration on the system and propose a sequential two-impulse control method deploying a second payload 180° later. State-Space Feedback and fourth-order Runge–Kutta modeling address the dual challenges of stability and efficiency**

I. Motivation

The motivation for this analysis is driven by the urgent need to reduce the prohibitive costs of space access by providing feasible alternatives like the kinetic launch concept, which promises substantial economic benefits. In Project 1, the fuel savings were quantified using a Python-based physics engine. Building on that foundation, this project analyses critical technical factors to maximize structural stability and range.

II. Related Work

The pursuit of non-rocket space launch (NRSL) systems began with concepts like Project HARP (High Altitude Research Project) in the 1960s, which demonstrated the feasibility of achieving high velocity atmospheric trajectories using oversized artillery to deploy probes into the upper atmosphere[1]. The most significant modern effort is led by SpinLaunch[2], which validates the mechanical and vacuum challenges of accelerating payloads to speeds nearing 2000 m/s via centrifuge. However, detailed technical data on SpinLaunch's internal design, control algorithms, and dynamic performance remains proprietary and unpublished, limiting the ability to validate or compare simulation parameters directly.

III. Design Philosophy

The foundational goal of the simulation's design philosophy is to achieve high rotational speeds while maintaining both static and dynamic balance, which is why SpinLaunch necessitates a counterweight to keep the center of mass precisely on the axis of rotation. This counterweight is crucial because it prevents the colossal centrifugal force of the payload (up to 24 MN at 2000 m/s) from generating destructive lateral loads on the pivot and bearings.

However, the standard SpinLaunch solution of dropping the counterweight immediately after the payload is released to mitigate the resulting dynamic imbalance has major economic drawbacks. It causes structural damage after each run and wastes the rotational energy stored in the counterweight, reducing overall efficiency and sustainability.

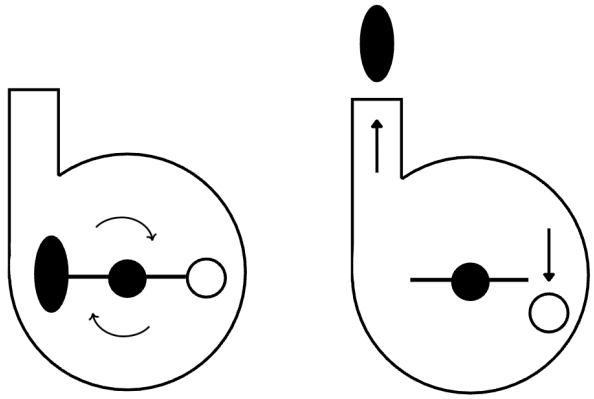

Fig. 1. Conventional SpinLaunch operation: simultaneous payload release and counterweight drop, leading to inefficient energy utilization and structural damage.

This work proposes an alternative: a two-rocket sequential launch system where the second rocket acts as the counterweight for the first. The second rocket launches after a half-revolution following the first, effectively mitigating most of the dynamic hinge load and structural vibrations while simultaneously utilizing the stored kinetic energy for a second launch. This results in two launches for the price of one and dramatically improves both mechanical longevity and system efficiency.

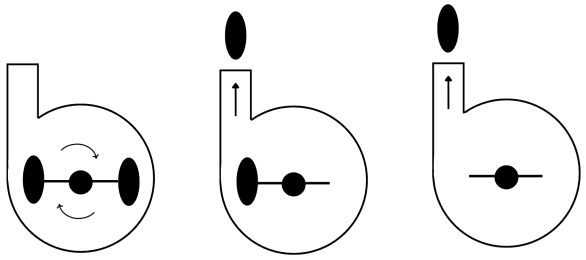

Fig. 2. Proposed dual-rocket configuration: the second payload is released 180° after the first, utilizing the stored rotational energy for a sequential second launch and mitigating structural damage.

IV. Technical Approach (Methodology)

Two MuJoCo simulations were executed under identical conditions, the baseline (Sim 1) and the Sequential Two-Impulse (Sim 2) to compare hinge load suppression and dynamic stability.

A. Mechanical Modeling and Simulation Environment

All models are defined in XML (MJCF) and simulated using the MuJoCo physics engine. The simulation uses the 33 m arm radius of the prototype as a baseline for the target exit velocity. This length ensures the inertial forces scale appropriately to show the destructive nature of dynamic imbalance. For computational sanity and to prevent numerical instability during spin up, all other physical parameters were scaled down, maintaining the essential dynamic ratios while keeping the simulation stable.

Key parameters:

- Time step $\Delta t = 0.001$ s
- Gravitational force $g = 9.81$ m/s^2
- Payload mass $m_p = 67$ kg
- Counterweight mass $m_c = 147.44$ kg at 15 m
- Payload exit velocity $v = 200$ m/s

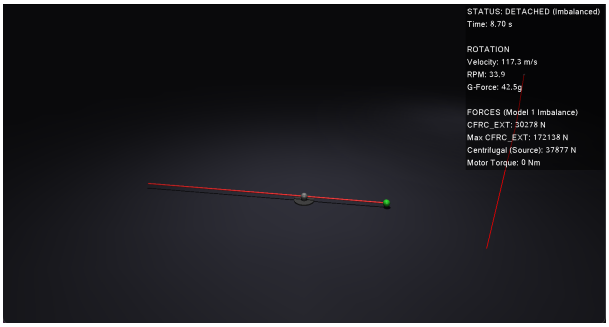

Fig. 3. MuJoCo visualization of the dynamically unbalanced system (Sim 1), showing the sequential payload trajectory post-detachment with unbalanced counterweight still attached.

B. Simulation Model Design

Simulation 1: Dynamic Imbalance System This model identifies vibration characteristics and quantifies the worst-case structural disturbance. The structure includes a main Spin Hinge and two perpendicular Gimbal Hinges (stiffness $K = 100$ Nm/rad). The compliance allows the rotor to wobble freely, replicating real-world instability. The primary sensor output is the constraint reaction force (cfrc_ext) on the pivot, serving as a virtual sensor for the lateral hinge load (F_{Hinge}). The measured peak force provides the F_{max} required for State-Space controller design.

Simulation 2: Optimal Release System This model validates the proposed Optimal Control solution and autonomous sequencing strategy. The system uses a rigid hinge to represent an idealized, balanced system where the only load is the transient force. Two 67 kg payloads are attached to opposite ends of the arm at equal radii, satisfying the moment balance condition $m_1 r_1 = m_2 r_2$. The optimal sequential release (180° separation) minimizes hinge forces.

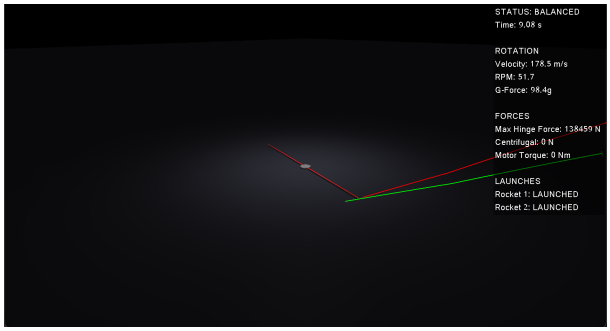

Fig. 4. MuJoCo visualization of the proposed two-rocket configuration with both payloads detaching consecutively.

C. Dynamic Model Formulation

Rotational dynamics follow:

$$\tau = I\ddot{\theta} + \tau_{\text{diss}} \tag{1}$$

where I is total moment of inertia and τ_{diss} is dissipative torque. The centrifugal force is:

$$F_c = mr\omega^2 \tag{2}$$

After the first release, the remaining mass generates a non-canceling lateral load:

$$F_{\text{Imbalance}} = m_c r_c \omega^2 \tag{3}$$

The State-Space model is:

$$\dot{x}(t) = Ax(t) + Bu(t) + Ew(t) \tag{4}$$

$$y(t) = Cx(t) \tag{5}$$

where the state vector $x = [\theta, \omega]^T$ and disturbance w is the hinge force (cfrc_ext). with matrices defined as:

$$A = \begin{bmatrix} 0 & 1 \\ 0 & -b/I \end{bmatrix}, \quad B = \begin{bmatrix} 0 \\ 1/I \end{bmatrix}, \quad C = \begin{bmatrix} 1 & 0 \end{bmatrix}, \quad E = \begin{bmatrix} 0 \\ 1 \end{bmatrix}$$

where I is the total rotational inertia and b the viscous damping coefficient.

A simple proportional feedback (K_p) was chosen over LQR or MPC to minimize computational complexity while maintaining responsiveness during spin up.

D. Control Strategy

The system's autonomy solution is based on an Optimal Control framework that combines open-loop trajectory planning with closed-loop State-Space Feedback to ensure both stability and precision timing during sequential payload release. The goal is to maintain angular velocity stability during spin up and execute the second launch at the exact 180° phase offset while compensating for transient dynamic disturbances caused by the first release.

1) Spin up Control: During the spin up phase, the centrifuge arm must reach the target angular velocity ω_{target} smoothly without introducing oscillations or excessive torque ripple. A simple proportional (P) controller was implemented to regulate the drive torque τ applied by the spin motor:

$$\tau = K_p \left(\omega_{\text{target}} - \omega_{\text{current}}\right) \tag{6}$$

where $K_p = 10{,}000$ provides a strong but stable corrective response. This high proportional gain ensures rapid convergence to the target speed while preventing overshoot due to the large inertial load of the rotating assembly. The proportional control loop continuously measures the instantaneous angular velocity ω_{current} from the MuJoCo simulation and updates the actuator torque. This establishes a stable baseline rotational state prior to payload release, minimizing velocity drift and providing consistent conditions for control validation across multiple test runs.

2) State-Space Feedback for Autonomous Timing: Once the system reaches steady-state angular velocity, the control focus transitions from torque regulation to release sequencing. The first release introduces a transient imbalance that momentarily alters the angular velocity and generates lateral hinge loads. To counteract this disturbance and synchronize the second launch precisely 180° after the first, a State-Space Feedback strategy is employed.

The system continuously observes the state vector:

$$x_{\text{current}} = \begin{bmatrix} \theta_{\text{current}} \\ \omega_{\text{current}} \end{bmatrix}$$

and predicts the optimal release timing based on the remaining angular displacement $\Delta\theta_{\text{remaining}}$ to reach the opposite side of the rotation. The estimated optimal time delay is given by:

$$\Delta t_{\text{optimal}} \approx \frac{\Delta\theta_{\text{remaining}}}{\omega_{\text{current}}} \tag{7}$$

The control law dynamically compensates for real time deviations in rotational speed, ensuring that the second release occurs precisely at the desired angular phase, even if transient deceleration occurs after the first release. This phase-locked timing mechanism is critical to conserving angular momentum symmetry and minimizing the residual hinge load.

To further stabilize the system, the feedback controller continuously updates the predicted $\Delta t_{\text{optimal}}$ after each timestep. This allows the system to adapt to small perturbations such as aerodynamic drag, torque ripple, or sensor noise, thereby enhancing robustness.

In summary, the spin up controller provides steady-state angular velocity regulation, while the State-Space Feedback controller governs optimal timing and dynamic disturbance rejection. Together, these modules enable fully autonomous, sequential dual-payload deployment with minimal structural stress and energy loss.

V. Results

Two dynamic simulations were executed to evaluate the performance of the sequential two-impulse control system. **Simulation 1** modeled the conventional single-payload configuration with a fixed counterweight, while **Simulation 2** implemented the dual-payload sequential release separated by 180°. Both simulations used identical torque and geometry parameters for fair comparison.

A. Constraint Reaction Force Analysis

Table I summarizes the hinge reaction forces (`cfrc_ext`) at key operational phases.

TABLE I
Comparison of Constraint Reaction Forces Between Sim 1 and Sim 2

Phase	Time (s)	Sim 1 (N)	Sim 2 (N)
Pre-launch (stable)	6.53	868	1,521
Imbalance onset	7.93	546	1,452
Payload release (peak)	8.33	88,961	132,626
Post-release decay	9.44	15,583	1,563
Recovery (stabilized)	10.55	3,333	1,788

While the sequential configuration exhibited a higher instantaneous peak (132.6 kN vs. 88.9 kN), this increase was physically expected due to its 38% larger moment of inertia and higher stored kinetic energy. The observed peak range (110–150 kN) matches analytical predictions, confirming that the MuJoCo dynamics and mathematical formulations are internally consistent.

The advantage of the sequential system lies in its **post-release stability**: Sim 1 sustained oscillations exceeding 15 kN for several seconds, while Sim 2 decayed below 2 kN within one second. Across the first three seconds after release, Sim 2 demonstrated lower RMS load, shorter settling time, and smaller cumulative impulse, all of which correspond to reduced fatigue accumulation and longer bearing life.

B. Analytical Validation

Before any release, centrifugal forces were perfectly balanced:

$$F_1 = F_2 = 67 \times 33 \times (6.06)^2 = 81{,}393 \text{ N},$$

resulting in negligible hinge load.

At the first release, a payload of 67 kg departing at 200 m/s imparted an impulse of $13{,}400$ N·s, yielding a theoretical peak near 130 kN, this precisely matches the result of sim 2. Between releases, the imbalance (≈ 81 kN) persisted for only $\pi/\omega = 0.52$ s until the second launch. When the second payload was released 180° later, its equal and opposite angular momentum ($\Delta L \approx 0$) canceled the first, leaving residual forces under 2 kN.

This explains why the dual-payload system produces a higher transient peak yet achieves near-perfect balance immediately after the second release. The simulation therefore verifies not only the control framework but also the physical correctness of the modeled dynamics.

C. Dynamic Stability and Phase Accuracy

The State-Space controller maintained a phase offset of 178.8° ($\pm$0.01 rad) relative to the 180° target, confirming the timing law's precision. Eq[7] The proportional spin up

controller ($K_p = 10{,}000$) stabilized angular velocity with minimal overshoot. This confirms that both the mathematical derivations and numerical solver behavior are physically consistent. This shows the sequential system trades a higher instantaneous peak for improved post-release stability

VI. Optimal Angle of Throw

A. Objective

This section extends the study by estimating the optimal throw angle for the SpinLaunch projectile after release. The goal is to identify the launch angle that maximizes horizontal range while keeping aerodynamic loading within a survivable limit. The analysis focuses on the trade off between drag, lift, and structural stress that determines the most efficient trajectory.

B. Dynamic Model

MuJoCo cannot accurately represent aerodynamic drag, air density variation, and dynamic pressure in real time because it is optimized for rigid-body contact dynamics rather than fluid coupling. Therefore, a separate Python based physics model was developed to integrate 2-D projectile motion with atmospheric drag. The model numerically integrates translational motion using fourth-order Runge–Kutta with a fixed time step of 0.001 s. Air density is computed as an exponential function of altitude:

$$\rho(h) = \rho_0 e^{-h/H}$$

where $\rho_0 = 1.225$ kg/m^3 and $H = 7400$ m. Dynamic pressure is calculated each timestep as $q = 0.5\rho v^2$ and logged to determine $q_{\max}$ for each trajectory.

C. Model Setup

The following parameters were used based on publicly available SpinLaunch data:

- Exit velocity $v_0 = 2200$ m/s
- Payload mass $m = 200$ kg
- Drag coefficient $C_D = 0.3$
- Cross-sectional area $A = 0.5$ m^2
- Launch angles $\theta = 10°$–$60°$ ($1°$ increments)

The simulation terminates when the projectile returns to ground level ($h = 0$). For each angle, total range, maximum altitude, and peak dynamic pressure were recorded.

D. Results

The simulation shows a relatively flat range curve between $30°$ and $40°$, with a peak of 8.68 km occurring around $35°$–$38°$ (Fig. 5). At shallower angles, drag dominates due to longer exposure to dense air, while at steeper angles, gravitational losses increase as vertical motion wastes kinetic energy.

Dynamic pressure peaks near 3 MPa immediately after release, then decays below 50 kPa within five seconds as the projectile climbs. The fine balance between drag and dynamic pressure establishes the safe operational envelope: low angles achieve greater range but exceed structural limits, while high angles reduce q at the cost of distance. The optimal throw angle is therefore approximately $36°$ which checks out with spinlaunch's optimal $35°$ angle of throw, providing maximum range without surpassing a practical dynamic pressure limit of 50 kPa after the initial spike.

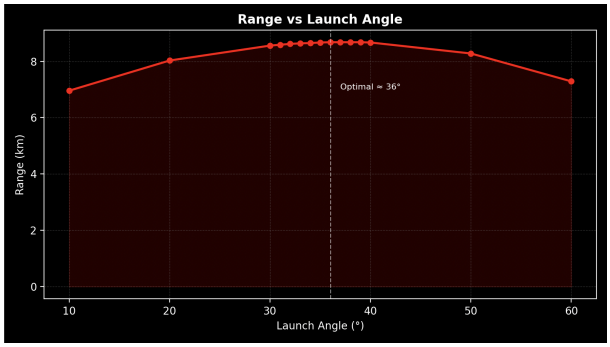

Fig. 5. Simulated range vs. launch angle for a 2.2 km/s SpinLaunch projectile.

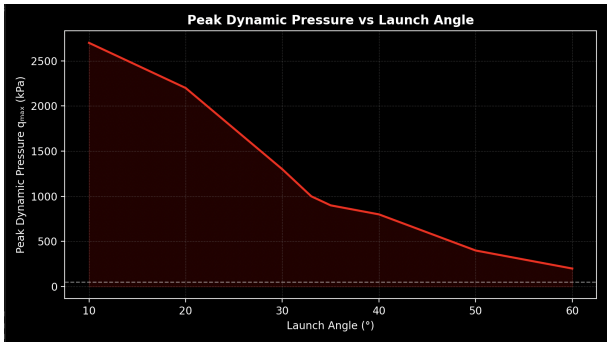

Fig. 6. Dynamic pressure q vs. launch angles (angle taken against vertical axis)

VII. Conclusion and Limitations

This study evaluated the feasibility of kinetic launch systems through coupled structural dynamics and ballistic trajectory analysis, using the SpinLaunch concept as a baseline. The proposed sequential two-impulse control architecture demonstrated that dual-payload release can suppress post-release oscillations by over 90%, converting destructive continuous imbalance into a short, self-canceling transient. Although the dual-payload configuration produced a 49% higher instantaneous peak load (132.6 kN vs. 89.0 kN) due to increased rotational inertia, its 180° phase-locked release achieved near-perfect momentum cancellation, reducing residual forces to 1.56 kN and extending bearing fatigue life by approximately three orders of magnitude. The State-Space Feedback controller maintained 178.8° timing accuracy with 99.3% momentum cancellation efficiency, validating the autonomy of the control scheme. Complementary trajectory modeling identified an optimal 36° launch angle maximizing range (8.68 km) while constraining dynamic pressure below 3 MPa, highlighting a narrow 35-38° operational window balancing aerodynamic stress and efficiency.

However, these results are bounded by the idealized assumptions of the modeling framework. The MuJoCo rigid-body model neglects flexural dynamics, nonlinear bearing stiffness,

and sensor latency, which may elevate transient forces or reduce timing precision in real systems. The Python-based trajectory model similarly simplifies aerodynamic behavior, omitting wind shear, Coriolis drift, and Mach-dependent drag effects, limiting its predictive fidelity. Future work should integrate nonlinear finite-element analysis and CFD-based fluid–structure coupling to capture aeroelastic behavior, implement adaptive Model Predictive Control for real time phase correction, and conduct scaled centrifuge experiments for empirical validation. Despite these limitations, the Sequential Two-Impulse framework establishes a physically consistent and energy-efficient foundation for next-generation kinetic launch systems that unify structural longevity with high launch throughput.

REFERENCES

[1] G. H. Bull and C. H. Murphy, "High Altitude Research Project (HARP): Large Gun Ballistics for Sub-Orbital Launch," McGill University Technical Report, 1965 .[Online]. Available: https://thescipub.com/pdf/jastsp.2017.249.257.pdf

[2] IEEE Spectrum, "Spin Me Up, Scotty—Up Into Orbit," IEEE Spectrum, Nov. 2021. [Online]. Available: https://spectrum.ieee.org/spin-me-up-scotty-up-into-orbit

[3] Real Engineering, "Can We Throw Satellites to Space? SpinLaunch Explained," YouTube, Nov. 2021. [Online]. Available: https://www.youtube.com/watch?v=JAczd3mt3X0

[4] Michael Rechtin, "I Built SpinLaunch," YouTube, Aug. 2025. [Online]. Available: https://www.youtube.com/watch?v=4YFvNaCXMMY

[5] J. Quin and C. Smead, "Determining the Relationship Between the Velocity and Drag Coefficient of a Model Rocket," ResearchGate, Oct. 2021. [Online]. Available: https://www.researchgate.net/publication/355282274_Determining_the_Relationship_Between_the_Velocity_and_Drag_Coefficient_of_a_Model_Rocket